Nature **338**, 553 (1989); H.-L. Lin, L. C. Peterson, J. T. Overpeck, S. E. Trumbore, D. W. Murray, *Paleoceanography* **12**, 415 (1997); G. H. Haug *et al.*, *Paleoceanography* **13**, 427 (1998).
3. L. C. Peterson, J. T. Overpeck, N. G. Kipp, J. Imbrie, *Paleoceanography* **6**, 99 (1991).
4. K. A. Hughen, J. T. Overpeck, L. C. Peterson, S. Trumbore, *Nature* **380** 51 (1996); K. A. Hughen *et al.*, *Nature* **391**, 65 (1998).
5. F. A. Richards, *Oceanogr. Mar. Biol. Annu. Rev.* **13**, 11 (1975); F. Muller-Karger and R. Aparicio-Castro, *Cont. Shelf Res.* **14**, 199 (1994).
6. M. D. de Miró, *Acta Geol. Hisp.* **6**, 102 (1971); K. A. Tedesco, R. C. Thunell, E. Tappa, F. Muller-Karger, R. Bohrer, *Eos* **78** (fall suppl.), F342 (1997).
7. Samples were washed through a 63-μm sieve and dried, and the >150-μm fractions were analyzed for their planktic foraminiferal content with a standard binocular microscope. A total of 564 samples, each 1 mm thick, were used in this study. All data are archived at www.ngdc.noaa.gov/paleo/paleo.html.
8. K. A. Hughen, J. T. Overpeck, L. C. Peterson, R. F. Anderson, in *Palaeoclimatology and Palaeoceanography from Laminated Sediments*, A. E. S. Kemp, Ed. (Geological Society Spec. Publ. No. 116, The Geological Society, London, 1996), pp. 171–183; D. E. Black, thesis, Univ. of Miami, Coral Gables, FL (1998).
9. C. K. Folland, T. N. Palmer, D. E. Parker, *Nature* **320**, 602 (1986). Interhemispheric SST anomalies were recalculated as North Atlantic SST anomalies minus South Atlantic SST anomalies.
10. P. Chang, L. Ji, H. Li, *Nature* **385**, 516 (1997).
11. A. D. Moura and J. Shukla, *J. Atmos. Sci.* **38**, 2653 (1981); J. Servain, *J. Geophys. Res.* **96**, 15137 (1991).
12. A. Kaplan *et al.*, *J. Geophys. Res.* **103**, 18567 (1998).
13. S. Hastenrath and L. Greischar, *J. Geophys. Res.* **98**, 5093 (1993).
14. W. M. Gray, *Science* **249**, 1251 (1990); Y. Kushnir, *J. Clim.* **7**, 141 (1994).
15. R. R. Dickson, J. Meincke, S. A. Malmberg, A. J. Lee, *Prog. Oceanogr.* **20**, 103 (1988); S. Levitus, *J. Geophys. Res.* **94**, 9679 (1990).
16. P. Schlosser, G. Bönisch, M. Rhen, R. Bayer, *Science* **251**, 1054 (1991); L. A. Mysack and S. B. Power, *Climatol. Bull.* **25**, 81 (1991).
17. R. J. Greatbatch, A. F. Fanning, A. D. Goulding, S. Levitus, *J. Geophys. Res.* **96**, 22009 (1991).
18. A. W. Robertson, C. R. Mechoso, Y. -J. Kim, *J. Clim.*, in press.
19. W. A. Sanchez and J. E. Kutzbach, *Quat. Res.* **4**, 128 (1974).
20. P. W. Glynn, E. M. Druffel, R. B. Dunbar, *J. Mar. Res.* **41**, 605 (1983).
21. A. Tarussov, in *Climate Since A.D. 1500*, R. S. Bradley and P. D. Jones, Eds. (Routledge, London, 1992), pp. 505–516; L. Koch, *Meddeleser om Grønland* **130** (Copenhagen) (1945); A. E. J. Ogilvie, *Acta Archaeol.* **61**, 233 (1991); ———, in *Climate Since A.D. 1500*, R. S. Bradley and P. D. Jones, Eds. (Routledge. London. 1992), pp. 92–117.
22. L. D. Keigwin, *Science* **274**, 1504 (1996).
23. A. E. Jennings and N. J. Weiner, *Holocene* **6**, 179 (1996).
24. W. Dansgaard *et al.*, *Nature* **255**, 24 (1975); L. K. Barlow *et al.*, *Holocene* **7**, 489 (1997).
25. L. L. Ely, Y. Enzel, V. Baker, D. R. Cayan, *Science* **262**, 410 (1993); M. K. Hughes and L. J. Graumlich, in *Climatic Variations and Forcing Mechanisms of the Last 2000 Years*, P. D. Jones, R. S. Bradley, J. Jouzel, Eds. (Springer-Verlag, Berlin, 1996), pp. 109–124; H. D. Grissino-Mayer, in *Tree Rings, Environment, and Humanity*, J. S. Dean, D. M. Meko, T. W. Swetnam, Eds. (Radiocarbon, University of Arizona, 1996), pp. 191–204.
26. K. R. Laird, S. C. Fritz, K. A. Maasch, B. F. Cumming, *Nature* **384**, 552 (1996); K. R. Laird, S. C. Fritz, B. F. Cumming, *J. Paleolimnol.* **19**, 161 (1998).
27. C. A. Woodhouse and J. T. Overpeck, *Bull. Am. Meteorol. Soc.* **79**, 2693 (1998).
28. The spectral analysis was done with the methods of M. E. Mann and J. M. Lees [*Clim. Change* **33**, 409 (1996)]. The power spectrum for the pre-1900 pre-industrial series was nearly identical to that of the complete record.
29. U. Mikolajewicz and E. Maier-Reimer, *Clim. Dyn.* **2**, 63 (1990); S. Manabe and R. J. Stouffer, *J. Clim.* **9**, 376 (1996); T. Delworth, S. Manabe, R. J. Stouffer, *Geophys. Res. Lett.* **24**, 257 (1997); A. Timmerman and M. Latif, *J. Clim.* **11**, 1906 (1998).
30. M. E. Mann and J. Park, *J. Geophys. Res.* **99**, 25,819 (1994); V. M. Mehta and T. Delworth, *J. Clim.* **8**, 172 (1995).
31. M. E. Schlesinger and N. Ramankutty, *Nature* **367**, 723 (1994).
32. M. E. Mann, J. Park, R. S. Bradley, *Nature* **378**, 266 (1995); M. E. Mann, R. S. Bradley, M. K. Hughes, *Nature* **392**, 779 (1998).
33. M. Stuiver and P. D. Quay, *Science* **207**, 11 (1980).
34. D. Rind and J. T. Overpeck, *Quat. Sci. Rev.* **12**, 357 (1993).
35. M. Stuiver and T. F. Braziunas, *Radiocarbon* **35**, 137 (1993).
36. S. D. Woodruff, R. J. Slutz, R. L. Jeanne, P. M. Steurer, *Bull. Am. Meteorol. Soc.* **68**, 1239 (1987).
37. Funded by NSF and the National Oceanic and Atmospheric Administration. We thank C. Rooth, M. Mann, P. Chang, and J. Cole for valuable discussions. This is a contribution from the Rosenstiel School of Marine and Atmospheric Science, University of Miami.

13 July 1999; accepted 19 October 1999

---

van der Waals Interactions in the Cl + HD Reaction

Dimitris Skouteris,[1] David E. Manolopoulos,[1] Wensheng Bian,[2] Hans-Joachim Werner,[2] Lih-Huey Lai,[3] Kopin Liu[3]

The van der Waals forces in the entrance valley of the Cl + HD reaction are shown here to play a decisive role in the reaction's dynamics. Exact quantum mechanical calculations of reactive scattering on a potential energy surface without Cl–HD van der Waals forces predict that the HCl and DCl products will be produced almost equally, whereas the same calculations on a new ab initio potential energy surface with van der Waals forces show a strong preference for the production of DCl. This preference is also seen in crossed molecular beam experiments on the reaction. The study of chemical reaction dynamics has now advanced to the stage where even comparatively weak van der Waals interactions can no longer be neglected in calculations of the potential energy surfaces of chemical reactions.

The idea that the structure of the transition state of a chemical reaction determines the overall thermal rate coefficient is deeply ingrained in our understanding of chemical reactions, and it forms the basis of a number of approximate (*1*) and exact (*2*) theories of chemical reaction rates. However, there is no indication from these theories that the more detailed dynamics of chemical reactions will not be sensitive to regions of the potential energy surface that are far removed from the transition state region, such as the shallow wells in the reactant and product valleys that are caused by van der Waals interactions. Here we show that the van der Waals forces in the entrance valley of the Cl + HD reaction do in fact have a substantial effect on the outcome of this reaction when the HD molecule is rotationally unexcited. This result has some precedent in the context of ion-molecule reactions, the rates of which are often dominated by long-range electrostatic forces and can be highly sensitive to the initial rotational state of the reactant molecule (*3*). However, ion-molecule reactions often proceed without activation barriers, whereas the Cl + HD reaction is a classic example of an activated chemical reaction (*4*). Furthermore, the van der Waals forces in the entrance valley of the Cl + HD reaction are considerably weaker than the long-range forces in ion-molecule reactions. For example, the depth of the Cl–HD van der Waals well is less than one-tenth the height of the reaction barrier on the Cl + HD potential energy surface (Fig. 1). The fact that such weak van der Waals forces can actually affect the outcome of the reaction is quite remarkable.

The kinetics of the Cl + H_2 reaction and its deuterium-substituted isotopomers have been studied for well over a century. The reaction played a central role in the development of transition state theory (*4*), is an important elementary step in the mechanism of the $Cl_2 + H_2 \rightarrow 2HCl$ chain reaction (*5*), and has been used as a textbook example of the kinetic isotope effect (*6*). A number of electronic potential energy surfaces have been developed for the reaction over the years, the most recent being the G3 potential energy surface of Truhlar *et al.* (*7*). This surface has been shown in variational transition state theory (VTST) calculations (*7*) to give excellent overall agreement with experimental thermal rate coefficients (*8*) for the Cl + H_2 and Cl + D_2 reactions over a wide temperature range. Furthermore, detailed quasi-

---

[1] Physical and Theoretical Chemistry Laboratory, South Parks Road, Oxford OX1 3QZ, UK. [2] Institute für Theoretische Chemie, Universität Stuttgart, Pfaffenwaldring 55, D-75069 Stuttgart, Germany. [3] Institute of Atomic and Molecular Sciences, Academia Sinica, Post Office Box 23-166, Taipei, Taiwan 10764.

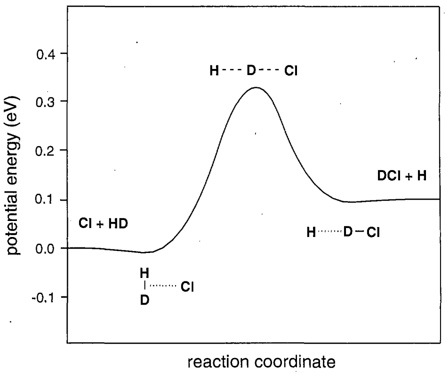

Fig. 1. Schematic reaction profile for the Cl + HD → DCl + H reaction on the BW potential energy surface of (*15*).

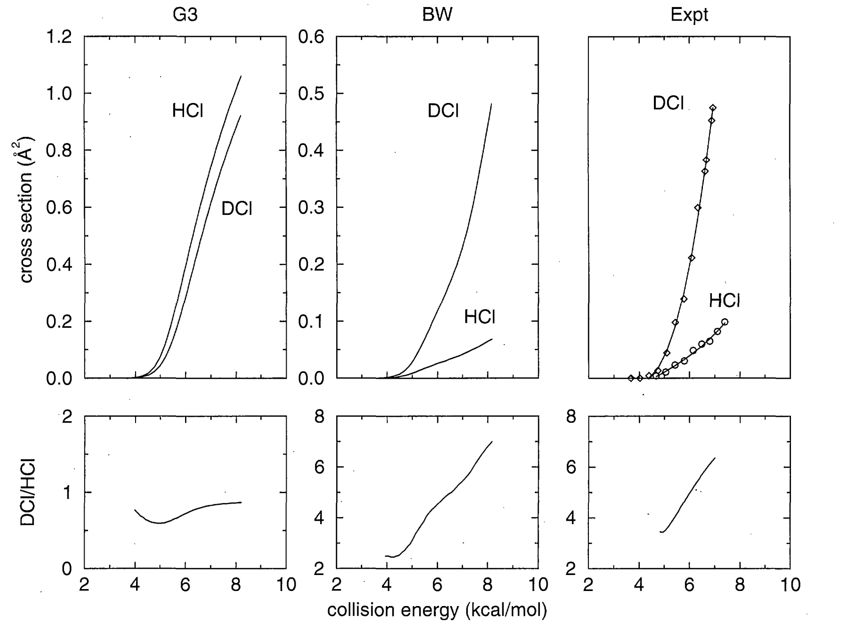

Fig. 2. Comparison of theoretical and experimental excitation functions and DCl/HCl product branching ratios for the Cl + HD(v = 0, 82% j = 0 + 18% j = 1) reaction. The top three panels show the cross sections for DCl and HCl production as a function of the collision energy. The bottom three panels show the corresponding DCl/HCl product branching ratios. The columns labeled G3 and BW show the results of the calculations on the two different potential energy surfaces, whereas the column labeled Expt shows the relative cross sections for HCl and DCl production that were measured in the present molecular beam experiment.

classical trajectory (QCT) and quantum mechanical (QM) reactive scattering calculations on the G3 potential energy surface have been found to be in good agreement with the HCl product angular distributions measured in molecular beam experiments (*9*). However, although both of these experimental results are clearly sensitive to the shape of the potential energy surface in the transition state region, they are comparatively insensitive to the potential in the reactant valley.

In order to provide a more sensitive test of the reactant valley region, we performed a crossed molecular beam experiment on the Cl + HD isotopomer of the reaction using the procedures described in (*10*). In brief, a Cl atom beam was generated by 355-nm laser photolysis of Cl_2 at the throat of a pulsed valve. The subsequent supersonic expansion and skimming served to cool and confine the Cl beam, which then collided with the target HD beam from a second pulsed valve. The photodissociation of Cl_2 at 355 nm yields only about 1% of the excited spin-orbit state of the Cl atom (*11*), and therefore only the ground spin-orbit state contributed to the experimental measurements. The characterization of the HD beam indicated an average rotational energy of 0.05 kcal/mol, which corresponds to a rotational temperature of 50 K with 82% of the HD in its ground rotational state (j = 0) and the remaining 18% in j = 1. All of the reactant HD molecules were in their ground vibrational state (v = 0). The reaction excitation function (that is, the translational energy dependence of the reaction cross section) was measured for each of the two product channels using the procedures described in (*10*). The uncertainties in the relative cross sections for the two channels were determined to be within ±5%, and the overall errors in the experiment, including uncertainties in the collision energy, were estimated to be less than ±10%.

The results of this molecular beam experiment were then compared with QM calculations of reactive scattering on the G3 surface (Fig. 2). These calculations were performed with the use of the same hyperspherical coordinate reactive scattering methods that were used previously to study the dynamics of the F + H_2 and F + HD reactions (*12*). In the present application to the Cl + HD reaction, all reactant and product channels with diatomic rotational quantum numbers less than or equal to j_{max} = 17, helicity quantum numbers less than or equal to k_{max} = 3, and internal energies within E_{max} = 1.7 eV of the bottom of the asymptotic reactant valley were included in the QM basis set, resulting in over 850 coupled channels for the largest angular momentum and parity blocks involved. The calculations were performed at 26 total energies between 0.35 and 0.60 eV, and for all total angular momentum quantum numbers up to J_{max} = 35. Numerous convergence tests were performed to check the accuracy of the calculations, which were determined to be converged to within ±5% for all of the results presented here.

The theoretical results in Fig. 2 consist of absolute excitation functions for the Cl + HD → HCl + D and Cl + HD → DCl + H reactions, along with the corresponding DCl/HCl product branching ratios. The experimental results consist of relative excitation functions for the two reactions, because it was not possible to determine absolute reaction cross sections in the molecular beam experiment. The collision energy dependence of the DCl/HCl product branching ratio was, however, extracted from the experiment in order to provide a direct comparison with the results of the calculations. It was clear from this comparison that, in spite of its promising agreement with earlier experiments (*7*, *9*), the G3 potential energy surface substantially underestimated the measured DCl/HCl product branching ratio throughout the entire experimental collision energy range.

This disagreement between theory and experiment motivated the development of a new ab initio potential energy surface for the Cl + H_2 reaction by Bian and Werner (BW), the computed cross sections for which are also shown in Fig. 2. The new surface was constructed with the use of quantum chemical techniques (*13*) similar to those used previously to construct the Stark-Werner potential energy surface for F + H_2 (*14*, *15*). The calculated cross sections on this new surface were found to improve the agreement with the present Cl + HD experiment and reproduce the experimental preference for the DCl product very well (Fig. 2).

The transition state regions of the BW and G3 surfaces are broadly similar. Both surfaces have collinear transition states, with classical barrier heights of 7.61 and 7.88 kcal/mol, respectively (*16*). The harmonic vibrational frequencies for the bending and stretching coordinates at the transition state are also very similar at 540 and 1360 cm^{-1} for BW and 581 and 1358 cm^{-1} for G3. There is a notable difference, however, in the imaginary frequencies, which are 1294i cm^{-1} for BW and 1520i cm^{-1} for G3, indicating that the G3 surface has a

Table 1. Thermal DCl/HCl product branching ratios for the Cl + HD reaction.

Temperature (K)	Theory			Experiment*
	G3 (VTST)†	G3 (QM)‡	BW (QM)‡	
300	0.49	0.51	0.38	0.57
445	0.56	0.54	0.47	0.73

*Experimental results from (*18*). †Variational transition state theory results from (*7*). ‡QM results from the present calculations.

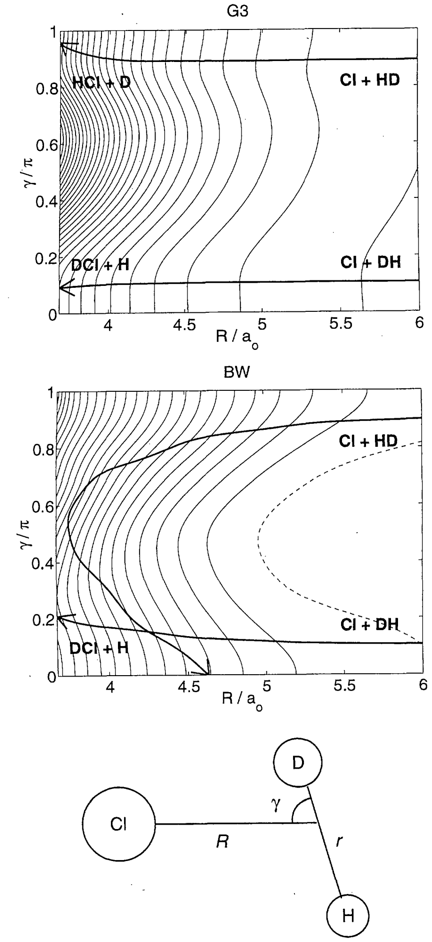

Fig. 3. Typical reactive classical trajectories leading to the HCl and DCl products on the G3 surface (top panel), compared with trajectories from the same Cl + HD(v = 0, j = 0) semiclassical initial conditions on the BW surface (middle panel). The thin lines in each panel are contours of the two-dimensional potential energy function $V(R,\gamma) = \min_r V(R,r,\gamma)$ in steps of 20 meV, with the first (dashed) line in the BW panel corresponding to an energy of −10 meV below the bottom of the asymptotic reactant valley. The coordinates R, r, and γ are defined in the bottom panel, and the scale of the R axes is in bohrs ($1a_0 = 5.29177 \times 10^{-11}$ m). The G3 surface is collinearly constrained throughout its entrance valley, whereas the BW surface has a Cl − HD van der Waals well with a nonlinear equilibrium geometry.

somewhat thinner barrier at collinear geometries. More important, the two surfaces have very different shapes in the reactant valley. The G3 surface has no van der Waals well and is most repulsive for perpendicular approach of the H_2 or HD to the Cl atom. In contrast, the BW surface is attractive at long distances and has a van der Waals minimum with a well depth of 0.5 kcal/mol at a T-shaped equilibrium geometry (Fig. 1). This is similar to the F + H_2 case and results from the dispersion and quadrupole-quadrupole interactions between the reactants. Moreover, the van der Waals interactions are not confined to the well region but persist for some distance into the side of the reaction barrier.

In order to understand how these differences between the two potential energy surfaces lead to the calculated QM cross sections in Fig. 2, we used a simple classical mechanical model. This is justified by the fact that qualitatively similar product branching ratios are obtained on both potential energy surfaces when the calculations are performed with the QCT method (*17*). Reactive classical trajectories leading to the DCl and HCl products on the G3 surface were therefore compared with trajectories from the same initial conditions on the BW surface (Fig. 3). Approximately half of the trajectories that reacted to produce DCl on the G3 surface also reacted on the BW surface, despite the influence of the van der Waals forces in the reactant valley. However, most of the trajectories that reacted to produce HCl on the G3 surface were deflected by the torque toward perpendicular geometries in the entrance valley of the BW surface before reaching the transition state region, and subsequently exited the entrance valley without reacting.

Although this effect is only illustrated in Fig. 3 for two particular classical trajectories, we have found it to be quite general for trajectories with semiclassical initial conditions corresponding to Cl + HD(v = 0, j = 0 and 1). The BW surface is less reactive for these trajectories than is the G3 surface, because the van der Waals forces in its entrance valley deflect trajectories away from the collinear transition state saddle point, thereby inhibiting the reaction at low collision energies where there is only just enough energy to surmount the reaction barrier. This effect is more pronounced for the HCl product than for the DCl product, because the center of mass of HD is closer to the D atom, and thus the H atom experiences the van der Waals forces at a larger Cl-to-HD separation (as can be seen from the asymmetry with respect to $\gamma \rightarrow \pi - \gamma$ of the potential energy contours in Fig. 3). Hence, a simple classical explanation accounts for both the lower absolute cross sections on the BW surface and the computed DCl/HCl product branching ratios in Fig. 2.

It should, however, be stressed that this explanation applies only to trajectories with low HD rotational excitation, for which the initial kinetic energy in the γ coordinate in Fig. 3 is comparatively small. Trajectories with more rapid HD rotation are not deflected so strongly by the van der Waals forces, and an entirely different picture therefore emerges when one considers a thermal population of initial HD(j) states at temperatures in excess of 50 K. Indeed, the experimental DCl/HCl product branching ratio is less than 1 for the Cl + HD reaction at temperatures between 300 and 445 K (*18*), in stark contrast to the present molecular beam results. This is clearly a result of the participation of higher HD(j) states at these elevated temperatures, and in fact the present QM calculations on both surfaces predict a preference for the HCl product when these higher HD rotational states are taken into account.

This preference can be seen when one compares experimental and theoretical DCl/HCl product branching ratios at temperatures of 300 and 445 K (Table 1). Because the population of the excited spin-orbit state of the Cl atom is less than 3% at the higher of these two temperatures, the recently established reactivity of this state (*19*) is unlikely to play an important role. The good agreement between the earlier VTST results and the present fully QM results on the G3 potential energy surface suggests that the product branching ratios at these temperatures are determined almost entirely by the shape of the potential in the transition state region, because the VTST calculation only involves this region of the potential energy surface. The fact that on neither surface is the QM result in particularly good agreement with the experiment at 445 K therefore implies that more work needs to be done to understand the transition state region. Closely related calculations suggest that the solution may simply be to include the effect of the Cl atom spin-orbit interaction in the BW surface (*16*).

References and Notes

1. D. G. Truhlar, W. Hase, J. T. Hynes, *J. Phys. Chem.* **87**, 2664 (1983).
2. W. H. Miller, *Acc. Chem. Res.* **26**, 174 (1993).
3. D. C. Clary, *Annu. Rev. Phys. Chem.* **41**, 61 (1990); W. L. Hase, *Science* **266**, 998 (1994), and references therein.
4. J. O. Hirschfelder, H. Eyring, B. Topley, *J. Chem. Phys.* **4**, 170 (1936); A. Wheeler, B. Topley, H. Eyring, *J. Chem. Phys.* **4**, 178 (1936); S. Saito, *J. Chem. Phys.* **23**, 2465 (1955).
5. K. J. Laidler, *Chemical Kinetics* (HarperCollins, New York, ed. 3, 1987), section 8.3.
6. H. S. Johnston, *Gas Phase Reaction Rate Theory* (Ronald Press, New York, 1966), chap. 13.

7. T. C. Allison, G. C. Lynch, D. G. Truhlar, M. S. Gordon, *J. Phys. Chem.* **100**, 13575 (1996).
8. J. C. Miller and R. J. Gordon, *J. Chem. Phys.* **75**, 5305 (1981); *J. Chem. Phys.* **78**, 3713 (1983); *J. Chem. Phys.* **79**, 1252 (1983); S. S. Kumaran, K. P. Lim, J. V. Michael, *J. Chem. Phys.* **101**, 9487 (1994).
9. N. Alagia *et al.*, *Science* **273**, 1519 (1996).
10. Y.-T. Hsu, J.-H. Wang, K. Liu, *J. Chem. Phys.* **107**, 2351 (1997); S.-H. Lee and K. Liu, *Chem. Phys. Lett.* **290**, 323 (1998).
11. Y. Matsumi, K. Tonokura, M. Kawasaki, *J. Chem. Phys.* **107**, 1065 (1992); P. C. Samartzitis, B. L. G. Bakker, T. P. Rakitzis, D. H. Parker, T. N. Kitsopoulos, *J. Chem. Phys.* **110**, 5201 (1999).
12. J. F. Castillo, D. E. Manolopoulos, K. Stark, H.-J. Werner, *J. Chem. Phys.* **104**, 6531 (1996); D. E. Manolopoulos, *J. Chem. Soc. Faraday Trans.* **93**, 673 (1997); J. F. Castillo and D. E. Manolopoulos, *Faraday Discuss. Chem. Soc.* **110**, 119 (1998).
13. H.-J. Werner and P. J. Knowles, *J. Chem. Phys.* **89**, 5803 (1988).
14. K. Stark and H.-J. Werner, *J. Chem. Phys.* **104**, 6515 (1996).
15. W. Bian and H.-J. Werner, *J. Chem. Phys.*, in press. The BW surface that was used in the present calculations is surface number 2 (BW2) of this forthcoming paper.
16. When the effect of spin-orbit coupling is taken into account, the classical barrier height on the ground adiabatic Cl + H_2 surface will increase by approximately one-third of the Cl atom spin-orbit splitting (that is, by 0.84 kcal/mol, bringing the overall barrier height on the BW surface up to 8.45 kcal/mol). The shape of the barrier may also change slightly because of the different angular dependences of the three coupled diabatic surfaces that correlate with Cl(^2P) + H_2. This spin-orbit effect was not included in the present calculations, but recent thermal rate constant calculations for the Cl + H_2 reaction have shown, by including the effect as an energy shift, that the true barrier height is indeed likely to be close to 8.45 kcal/mol (U. Manthe, W. Bian, H.-J. Werner, *Chem. Phys. Lett.*, in press).
17. H. L. Tomlinson, unpublished calculations.
18. Y. Bar Yaakov, A. Persky, F. S. Klein, *J. Chem. Phys.* **59**, 2415 (1973).
19. S.-H. Lee and K. Liu, *J. Chem. Phys.*, in press.

20. We thank H. Tomlinson for preparing Fig. 2, J. Simons and M. Child for their comments on an early draft of the manuscript, and M. Brouard for helpful discussions. Supported by the United Kingdom Engineering and Physical Sciences Research Council, the Deutsche Forshungsgemeinschaft, the German Fonds der Chemischen Industrie, the National Science Council of Taiwan, and the Chinese Petroleum Corporation.

2 June 1999; accepted 19 October 1999

Ordered Bicontinuous Nanoporous and Nanorelief Ceramic Films from Self Assembling Polymer Precursors

Vanessa Z.-H. Chan,[1] James Hoffman,[2] Victor Y. Lee,[3]
Hermis Iatrou,[4] Apostolos Avgeropoulos,[4] Nikos Hadjichristidis,[4]
Robert D. Miller,[3] Edwin L. Thomas[1]*

Three-dimensional ceramic nanostructured films were produced from silicon-containing triblock copolymer films exhibiting the double gyroid and inverse double gyroid morphologies (space group *Ia3d*). A one-step room-temperature oxidation process that used ozonolysis and ultraviolet irradiation effected both the selective removal of the hydrocarbon block and the conversion of the silicon-containing block to a silicon oxycarbide ceramic stable to 400°C. Depending on the relative volume fraction of the hydrocarbon block to the silicon-containing block, either nanoporous or nanorelief structures were fabricated with calculated interfacial areas of ~40 square meters per gram and pore or strut sizes of ~20 nanometers.

The controlled fabrication of mesoporous inorganic materials is an area of burgeoning interest because of their important applications as selective membranes, next-generation catalysts, and photonic materials. In 1993, Monnier *et al.* (*1*) reported the formation of mesoporous silica by using surfactant templates (MCM materials). This approach has allowed access to various mesoporous structures but generally involves multistep processes and does not allow simple production of large-area continuous films (*2*). Nonsurfactant templates, such as block copolymers or complex sugars, have also been used, but these processes again either involve multistep preparations (*3*), long processing times such as drying for 15 to 20 days (*4*), high calcination temperatures (between 400° to 800°C) (*5*), or some combination of the above.

We have produced porous and relief ceramic nanostructures from self-assembling (template-free) block copolymer precursors, with a one-step, low-temperature technique. By careful selection of the relative volume fraction and phases, block copolymers can be used to produce precursor materials with a vast range of different symmetries and structures that allow nanostructures with highly ordered and complex pore or strut structures to be prepared (*6*). In addition, pore sizes, feature sizes, and spacings are also readily tailored either through blending of one or more homopolymers with the block copolymer or through control of molecular weight. A bifunctional oxidation process was used to both selectively remove a hydrocarbon block and convert a remaining silicon-containing block to a silicon oxycarbide ceramic. The resulting ceramic materials are either nanoporous [three-dimensional (3D) connected pores] or nanorelief (3D connected strut networks), depending solely on the volume fraction of the hydrocarbon block relative to the silicon-containing block in the block copolymer precursor.

The formation of porous and relief nanostructures was accomplished by using two triblock copolymer precursors with compositions chosen to exhibit the double gyroid (*7*) and inverse double gyroid morphologies (space group *Ia3d*) (Fig. 1). This morphology was chosen because it allowed the production of intricate ceramic nanostructures with periodicities in three dimensions that are not obtainable by conventional lithographic techniques because of the small size and complexity of the patterns formed. The materials are triblock copolymers of the type A_1BA_2, where A is polyisoprene (PI) and B is poly(pentamethyldisilylstyrene) [P(PMDSS)] (*8*, *9*). One material has a composition of 24/100/26 (kg/mol) and forms a double gyroid morphology of PI networks [volume fraction of PI (ϕ_{PI}) = 33%] in a matrix of P(PMDSS) [referred to as the P(PMDSS)-DG] and is a precursor for the nanoporous structure. The other material has a composition of 44/168/112 (kg/mol) and forms the inverse double gyroid morphology of P(PMDSS) networks [$\phi_{P(PMDSS)}$ = 51%] in a matrix of PI [designated PI-DG] and can be converted into a nanorelief structure.

Samples of the triblock copolymers (1 mm thick) were cast from toluene and cryo-microtomed at −90°C. The approximately 50- to 100-nm-thick sections were then picked up either onto 600-mesh Cu grids or onto ultrathin amorphous carbon films on 100-mesh copper grids, and the PI blocks were preferentially stained in vapors of a 4% osmium tetroxide–water solution for 2 hours. These sections were then characterized in the bright-field mode with a JEOL 2000 FX transmission electron microscope (TEM), operating at 200 keV. Imaging of the unannealed, as-cast material revealed that highly ordered microphase separation occurs in this system even without annealing. Annealing the 1-mm-thick samples for 1 week at 120°C resulted in single grains that were several tens of

---

[1] Department of Materials Science and Engineering, Massachusetts Institute of Technology, Cambridge, MA 02139, USA. [2] Mathematical Science Research Institute, Berkeley, CA, 94720, USA. [3] IBM Almaden Research Center, San Jose, CA 95120, USA. [4] Department of Chemistry, University of Athens, Athens, Greece.

*To whom correspondence should be addressed. E-mail: ellt@mit.edu

LINKED CITATIONS

- Page 1 of 1 -

You have printed the following article:

van der Waals Interactions in the Cl + HD Reaction

Dimitris Skouteris; David E. Manolopoulos; Wensheng Bian; Hans-Joachim Werner; Lih-Huey Lai; Kopin Liu

Science, New Series, Vol. 286, No. 5445. (Nov. 26, 1999), pp. 1713-1716.

Stable URL:

http://links.jstor.org/sici?sici=0036-8075%2819991126%293%3A286%3A5445%3C1713%3AVDWIIT%3E2.0.CO%3B2-J

This article references the following linked citations:

References and Notes

[3] **Simulations of Gas-Phase Chemical Reactions: Applications to S_N 2 Nucleophilic Substitution**

William L. Hase

Science, New Series, Vol. 266, No. 5187. (Nov. 11, 1994), pp. 998-1002.

Stable URL:

http://links.jstor.org/sici?sici=0036-8075%2819941111%293%3A266%3A5187%3C998%3ASOGCRA%3E2.0.CO%3B2-5

[9] **Dynamics of the Simplest Chlorine Atom Reaction: An Experimental and Theoretical Study**

M. Alagia; N. Balucani; L. Cartechini; P. Casavecchia; E. H. van Kleef; G. G. Volpi; F. J. Aoiz; L. Bañares; D. W. Schwenke; T. C. Allison; S. L. Mielke; D. G. Truhlar

Science, New Series, Vol. 273, No. 5281. (Sep. 13, 1996), pp. 1519-1522.

Stable URL:

http://links.jstor.org/sici?sici=0036-8075%2819960913%293%3A273%3A5281%3C1519%3ADOTSCA%3E2.0.CO%3B2-N

NOTE: *The reference numbering from the original has been maintained in this citation list.*